Biochemistry

 Volume 41, Number 45 November 12, 2002

Current Topics

Impact of Enzyme Motion on Activity†

Sharon Hammes-Schiffer

Department of Chemistry, 152 Davey Laboratory, Pennsylvania State University, University Park, Pennsylvania 16802

Received August 23, 2002

ABSTRACT: Experimental and theoretical data imply that enzyme motion plays an important role in enzymatic reactions. Enzyme motion can influence both the activation free energy barrier and the degree of barrier recrossing. A hybrid theoretical approach has been developed for the investigation of the relation between enzyme motion and activity. This approach includes both electronic and nuclear quantum effects. It distinguishes between thermally averaged promoting motions that influence the activation free energy barrier and dynamical motions that influence the barrier recrossings. Applications to hydride transfer in liver alcohol dehydrogenase and dihydrofolate reductase resulted in the identification and characterization of important enzyme motions. These applications have also led to the proposal of a network of coupled promoting motions in enzymatic reactions. These concepts have important implications for protein engineering and drug design.

The relation between enzyme motion and activity has been probed with a variety of experimental techniques. High-resolution crystal structures for intermediates along enzymatic reaction pathways have provided evidence of substantial conformational changes (*1*). NMR experiments have been used to identify dynamic regions both in the active sites and far from the active sites of enzymes (*2*−*4*). These dynamic regions have been found to change along the enzymatic reaction pathway. In addition, kinetic measurements on mutant enzymes have shown significant changes in the catalytic rate for mutations both in the active site and far from the active site (*5*−*7*). Furthermore, double mutations exhibit nonadditive effects (*8*, *9*) [i.e., the effect of the double mutation is greater than the sum of the effects of the corresponding single mutations (*10*)], suggesting coupling between distal regions of the enzyme. These experimental observations imply that enzyme motion is a significant factor in enzymatic reactions.

Theoretical simulations of enzymatic reactions have provided further insight into the role of enzyme motion (*11*−*16*). In general, a chemical reaction in the condensed phase may be described in terms of a free energy profile as a function of a collective reaction coordinate. The overall rate may be expressed as the product of an equilibrium transition state theory rate, which is directly related to the activation free energy barrier, and the transmission coefficient, which accounts for dynamical recrossings of the barrier. Within this framework, the enzyme motion can influence the reaction in two distinct ways (*17*, *18*). First, the motion can influence the activation free energy barrier (i.e., the equilibrium between the top of the barrier and the reactant). These motions are thermally averaged, equilibrium properties of the system. Second, the motion can influence the recrossings of the free energy barrier. These motions are nonequilibrium dynamical properties of the system. Figure 1 depicts a schematic representation of a free energy profile with a trajectory that exhibits recrossings of the barrier.

For clarification, we define the terminology used in this review. The term "dynamics" is reserved for motions that influence the transmission coefficient (i.e., the barrier recrossings). The term "promoting motions" is defined as systematic changes in thermally averaged equilibrium prop-

† This work was supported by National Institutes of Health Grant GM56207 and National Science Foundation Grant CHE-0096357.

10.1021/bi0267137 CCC: $22.00
Published on Web 10/11/2002

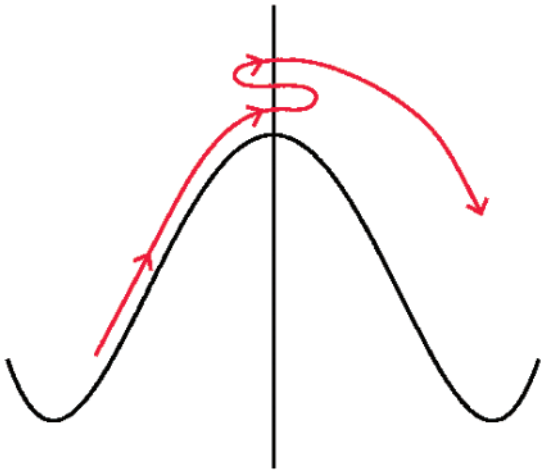

FIGURE 1: Schematic illustration of a free energy profile as a function of a collective reaction coordinate. The dividing surface is represented by the vertical line passing through the top of the barrier. The trajectory that is shown exhibits two forward recrossings of the dividing surface. This type of barrier recrossing is a dynamical effect and decreases the transmission coefficient.

erties along the collective reaction coordinate (i.e., as the reaction evolves from the reactant to the product). Promoting motions influence the activation free energy barrier, but they are not dynamical effects since they do not influence the transmission coefficient. Note that this definition does not differentiate between motions playing an active role in catalysis and motions simply responding to alterations caused by catalysis.

A promoting motion is fundamentally different from a promoting vibration, which has previously been defined as a geometrical change that occurs on a sub-picosecond time scale (*14*). Promoting motions are averaged over these fast vibrations of the enzyme and occur on the much longer time scale of the catalyzed chemical reaction. These promoting motions reflect the conformational changes that occur during the chemical reaction. The structures for the reactants and intermediates provide insight into these conformational changes. To fully understand the role of motion in enzymatic reactions, however, theoretical tools must be developed to elucidate the mechanisms by which these structural changes occur.

We have developed a hybrid theoretical approach for investigating the relation between enzyme motion and activity (*17*, *18*). This hybrid approach includes both electronic and nuclear quantum effects. It allows us to distinguish between thermally averaged promoting motions that influence the activation free energy barrier and dynamical motions that influence the barrier recrossings. This hybrid approach has been utilized to investigate hydride transfer in liver alcohol dehydrogenase (LADH) (*18*) and dihydrofolate reductase (DHFR) (*16*, *19*). The hydride transfer reactions catalyzed by these enzymes are depicted in Figure 2. These two applications will be used in this review to illustrate the fundamental principles of promoting and dynamical motions.

Quantum Mechanical Effects

Electronic quantum effects play an important role in enzymatic reactions. For example, the breaking and forming of chemical bonds require a substantial rearrangement of electrons. In addition, enzymatic reactions often result in a redistribution of electronic charge, particularly for charge transfer reactions such as proton or hydride transfer. This charge redistribution has a substantial impact on the electrostatic interactions within the system and often leads to reorganization of the enzyme during the reaction. Furthermore, some enzyme reactions are photoexcited and hence involve electronically excited states. The applications discussed in this review, however, are electronically adiabatic and hence remain in the electronic ground state.

In the hybrid approach described in ref *17*, the electronic quantum effects are incorporated with an empirical valence bond (EVB) potential. The EVB method describes a reaction in terms of a small number of valence bond states (*20*). For example, a simple hydride transfer reaction is described in terms of two valence bond states: state 1 has the hydride bonded to the donor (D−H A), and state 2 has the hydride bonded to the acceptor (D H−A). The Hamiltonian matrix elements between these valence bond states are represented as molecular mechanical terms fitted to electronic structure calculations or experimental data.

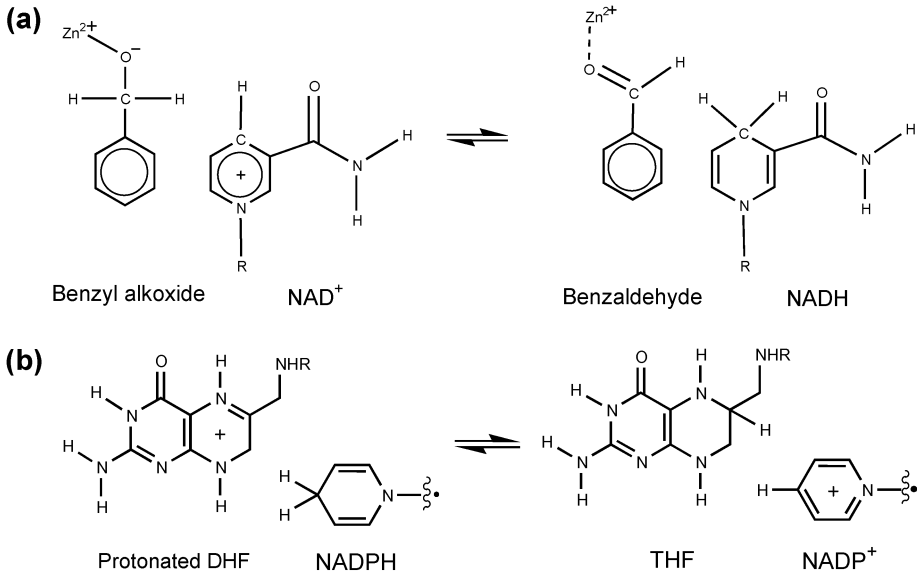

FIGURE 2: Schematic illustration of the hydride transfer reactions catalyzed by (a) LADH and (b) DHFR.

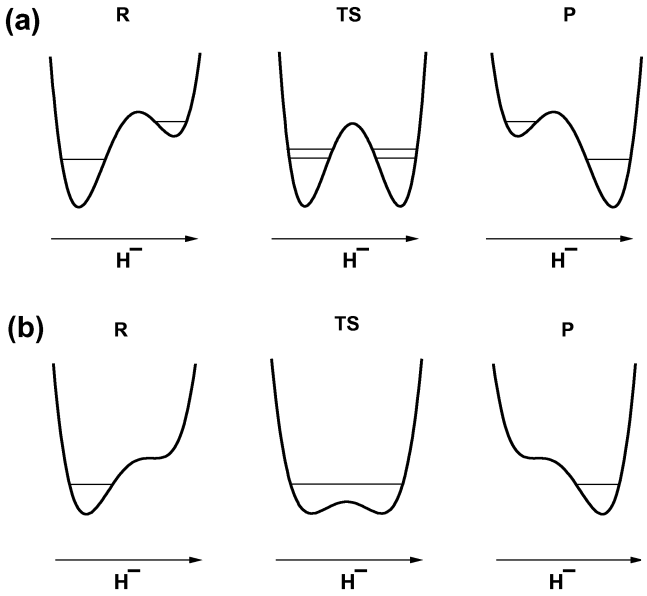

FIGURE 3: Schematic illustration of the one-dimensional hydride potential energy curves and the associated energies of the hydrogen vibrational states for two different hydride transfer reactions. The curves are functions of the one-dimensional hydride coordinate, and R, TS, and P correspond to the reactant, transition state, and product configurations, respectively. Panel a depicts hydride tunneling (i.e., the two lowest adiabatic vibrational states are below the barrier in the TS), and panel b depicts hydride transfer without tunneling (i.e., the lowest adiabatic vibrational state is above the barrier in the TS). Note that the intermediate configurations labeled TS need not be saddle points of the potential energy surface.

Nuclear quantum effects also play an important role in many enzymatic reactions, particularly those involving hydrogen transfer. The light mass of the hydrogen nucleus leads to nuclear quantum effects such as zero point energy and hydrogen tunneling. Figure 3 is a schematic illustration of nuclear quantum effects for two different types of hydride transfer reactions. This figure depicts the one-dimensional hydride potential energy curves and the associated energy levels for the hydrogen vibrational states along a collective reaction coordinate. The shape of the hydride potential energy curve is determined by the enzyme environment and thus changes along the collective reaction coordinate (i.e., as the reaction progresses). The donor well is lower in energy for the reactant, while the acceptor well is lower in energy for the product. The donor and acceptor wells are degenerate for the transition state. (Note that the intermediate configurations denoted as transition states in Figure 3 need not be saddle points on the potential energy surface but rather correspond to approximately symmetric double-well hydride potential energy curves.) In Figure 3a, the hydride transfer is a tunneling process since the two lowest adiabatic vibrational states are below the barrier in the transition state. The extent of tunneling is determined by the tunnel splitting (i.e., the energy separation between the adiabatic hydrogen vibrational states for the symmetric double-well potential). In contrast, in Figure 3b, the hydride transfer is no longer tunneling since the lowest adiabatic vibrational state is above the barrier in the transition state. Nevertheless, even in this case, the hydride transfer is still very much quantum mechanical in character.

The nuclear quantum effects can be included with a mixed quantum/classical method in which the transferring hydrogen

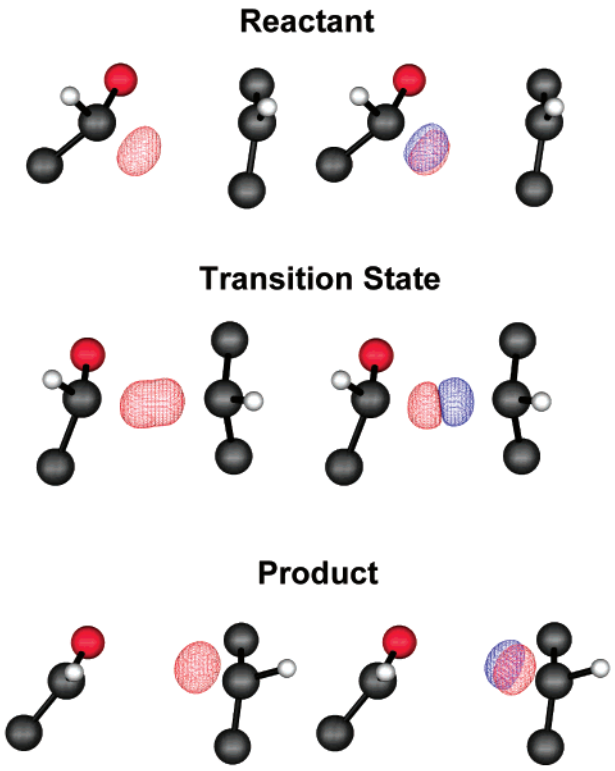

FIGURE 4: Vibrational wave functions of the transferring hydride for snapshots along the collective reaction coordinate of the LADH-catalyzed hydride transfer reaction. On the donor side, the alkoxide group and one carbon atom of the ring are shown, while on the acceptor side, the acceptor carbon atom and its first neighbors are shown. The ground and excited vibrational states are shown on the left and right, respectively.

nucleus is represented by a three-dimensional vibrational wave function, while the remaining nuclei are treated classically (*17*). We have developed the numerical methodology to calculate these hydrogen vibrational wave functions directly on a three-dimensional grid placed between the donor and acceptor (*21*, *22*). These hydrogen vibrational wave functions are calculated for each configuration of the classical nuclei sampled during the molecular dynamics simulation. Figure 4 depicts the three-dimensional hydrogen vibrational wave functions calculated for snapshots along the collective reaction coordinate for the hydride transfer reaction catalyzed by LADH (*18*). Note that the wave functions are localized near the donor (or acceptor) for the reactant (or product) configurations but are delocalized between the donor and acceptor for the transition state configuration. This delocalization arises from the symmetry of the hydride potential energy surface, as illustrated in the transition state one-dimensional potential energy curves in Figure 3.

Calculation of Rates

As mentioned above, the overall rate constant for a chemical reaction in the condensed phase may be written as

$$k_{dyn} = \kappa k_{TST} \quad (1)$$

Here k_{TST} is the equilibrium transition state theory rate constant

$$k_{TST} = \frac{k_B T}{h} \exp\left(\frac{-\Delta G^{\dagger}}{k_B T}\right) \quad (2)$$

where $\Delta G^{\dagger}$ is the activation free energy barrier for the reaction, k_B is Boltzmann's constant, h is Planck's constant, and T is temperature. The transition state theory rate constant is based on the assumption that the rate is determined by the forward flux through the dividing surface (*23*). (Typically, the dividing surface is chosen to correspond to the top of the free energy barrier, as shown in Figure 1.) Thus, transition state theory assumes that each trajectory passes through the dividing surface only one time. In dynamical systems, the environment may cause trajectories to recross the dividing surface. These types of barrier recrossings are illustrated in Figure 1. The prefactor κ is the transmission coefficient, which accounts for dynamical recrossings of the dividing surface (*24*).

In the hybrid theoretical approach (*17*), the free energy profile is calculated as a function of a collective reaction coordinate involving the entire solvated protein. This collective reaction coordinate is chosen to be the difference in energy between the two valence bond states (*17*, *20*). Thus, it is negative when the reactant state is lower in energy, positive when the product state is lower in energy, and zero when the reactant and product states are virtually degenerate. This reaction coordinate is analogous to the solvent reaction coordinate used in Marcus theory for electron transfer (*25*). Since the free energy barrier is often much larger than the thermal energy, a mapping (or umbrella) potential is used to drive the reaction over the barrier (*20*). This mapping potential is a linear combination of the two valence bond states. Individual pieces of the free energy profile are calculated along the collective reaction coordinate and are connected using thermodynamic integration. The nuclear quantum effects of the transferring hydrogen are included using an adiabatic perturbative approach. As shown in eq 2, the transition state theory rate constant may be calculated from the activation free energy barrier obtained from this adiabatic quantum free energy profile.

The transmission coefficient can be calculated with a reactive flux approach (*26*−*28*), where a large number of trajectories are initiated at the top of the barrier and are propagated backward and forward in time (*17*). Hydrogen transfer reactions may be vibrationally adiabatic or nonadiabatic, where adiabatic refers to reactions that remain in the ground vibrational state and nonadiabatic refers to reactions involving excited vibrational states. The effects of excited vibrational states can be included with a surface hopping approach (*29*, *30*), which is based on a probabilistic algorithm for including instantaneous nonadiabatic transitions according to the evolution of the time-dependent Schrödinger equation.

This hybrid approach provides information about the motions involved in enzymatic reactions. The promoting motions can be identified and characterized by analyzing the equilibrium adiabatic simulations utilized to generate the free energy profiles. Thermally averaged properties such as distances or angles may be calculated along the collective reaction coordinate. (These properties are weighted in an analogous manner as the contributions to the free energy profile.) The thermally averaged properties that exhibit systematic changes along the collective reaction coordinate are identified as promoting motions. These changes in average geometrical properties occur on the time scale of the hydride transfer reaction (i.e., milliseconds for DHFR). The individual simulations are propagated for only hundreds of picoseconds or tens of nanoseconds, but a series of such simulations are connected along the entire collective reaction coordinate in a way that provides information about the much longer time scale of hydride transfer. Note that the vibrations involving these distances and angles are typically on the subpicosecond time scale, but the *average* distances and angles change on the longer time scale of hydride transfer.

In addition, the dynamical motions may be identified and characterized by analyzing the real-time dynamical trajectories utilized to calculate the transmission coefficient. As discussed above, these trajectories are initiated at the transition state and propagated backward and forward in time. (The initial configurations at the transition state are obtained from equilibrium simulations with a biasing potential, and the trajectories are weighted accordingly.) These calculations provide nonequilibrium, real-time, dynamical information in the region of the transition state, typically on the femtosecond to picosecond time scale. The correlation between geometrical properties at the transition state and the degree of barrier recrossing may be calculated. Properties exhibiting a strong correlation with the barrier recrossing are identified as "dynamical motions". Note that promoting motions influence the activation free energy barrier (which is in the exponential of the rate expression), while dynamical motions influence the transmission coefficient (which is the prefactor of the rate expression). As a result, promoting motions are expected to have a greater impact on the enzymatic activity than dynamical motions.

Below, we summarize the applications of this hybrid theoretical approach to hydride transfer in the enzymes LADH and DHFR. Note that these types of simulations are challenging due to issues involving force fields and sampling. As a result, only the qualitative results are meaningful. In this review, these specific applications are being used to illustrate fundamental aspects of enzyme motion. These fundamental concepts are general and hence do not depend on the details of the specific systems.

Liver Alcohol Dehydrogenase

Liver alcohol dehydrogenase (LADH) catalyzes the reversible oxidation of alcohols to the corresponding aldehydes and ketones. This enzyme is critical to many steps in metabolism and is relevant to the medical complications associated with alcoholism. The kinetic isotope effects for this enzymatic reaction have been measured by Klinman and co-workers, who interpret the results as an indication of hydrogen tunneling (*31*, *32*). Numerous theoretical studies of this reaction have been performed (*33*−*38*).

This review will focus on the application of the hybrid approach described above to the LADH-catalyzed hydride transfer reaction depicted in Figure 2a (*18*). Both theory and experiment suggest that the proton transfer from the hydroxyl group of the alcohol substrate occurs prior to the hydride transfer (*39*). The resulting alkoxide is stabilized by the catalytic zinc. As shown in Figure 2a, the hydride is transferred from benzyl alkoxide to NAD^+ to form the products benzaldehyde and NADH.

The classical and adiabatic quantum free energy profiles as functions of the collective reaction coordinate are shown in Figure 5. The experimental free energy of reaction and

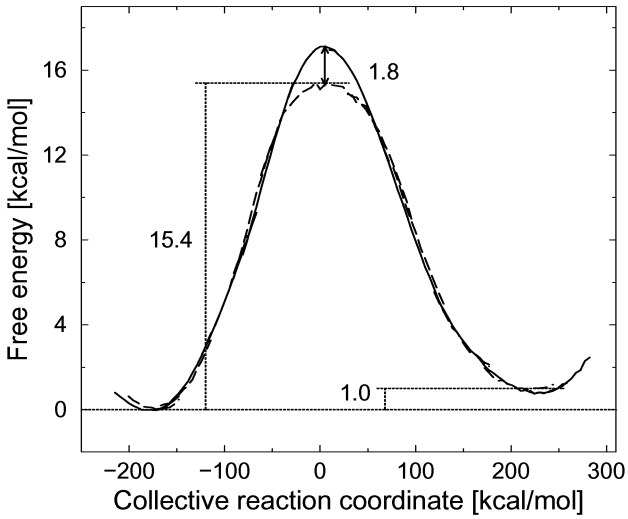

FIGURE 5: Free energy profiles of the LADH-catalyzed hydride transfer reaction as functions of the collective reaction coordinate. The solid line indicates the classical profile, and the dashed line indicates the adiabatic quantum profile (including zero point motion for the transferring hydride). The minimum free energies of the classical and adiabatic quantum profiles are set to zero, and the difference in free energy barriers is indicated. The dotted lines denote experimental values.

free energy of activation are reproduced as a result of fitting two EVB parameters. Note that the adiabatic quantum activation free energy profile is 1.8 kcal/mol lower than the classical activation free energy. This difference indicates that the nuclear quantum effects significantly influence the rate for this reaction. Analysis of the nuclear wave functions for configurations at the top of the free energy barrier (depicted as the transition state in Figure 4) suggests that hydrogen tunneling along the donor−acceptor axis is prevalent. The calculated deuterium and tritium kinetic isotope effects are in agreement with the experimental values. The transmission coefficient is calculated to be 0.95, suggesting that dynamical barrier recrossings are not important for this reaction.

We investigated the role of motion in the LADH reaction. Our studies focused on four properties: the donor−acceptor distance, the nicotinamide ring puckering angle, the zinc−oxygen distance, and the distance between $C_{\gamma 1}$ of Val-203 and the acceptor carbon atom. The thermally averaged properties along the collective reaction coordinate are depicted in Figure 6. As expected, the donor−acceptor distance decreases as the reaction evolves from the reactant to the transition state (defined as zero reaction coordinate). The out-of-plane angles in the NAD^+/NADH ring increase at the transition state, implying that the boat configuration is energetically more favorable than the chair configuration at the transition state. The monotonic increase in the zinc−oxygen distance is consistent with the decrease in the level of electrostatic interaction as the substrate is converted from an alkoxide to an aldehyde. More surprisingly, the distance between Val-203 $C_{\gamma 1}$ and the acceptor carbon increases as the reaction evolves from the reactant to the transition state, suggesting that the relative motion of Val-203 and the acceptor carbon contributes to the reaction coordinate. All of these properties are promoting motions and hence influence the activation free energy barrier.

We also investigated the dynamical effects of these motions by calculating the correlation between these properties at the transition state and the degree of dynamical barrier recrossing for a canonical ensemble of trajectories. The donor−acceptor distance and one of the out-of-plane ring angles of NAD^+/NADH were found to be correlated to the degree of barrier recrossing. Since the transmission coefficient is nearly unity, however, these nonequilibrium dynamical effects are not expected to play an important role for this enzyme.

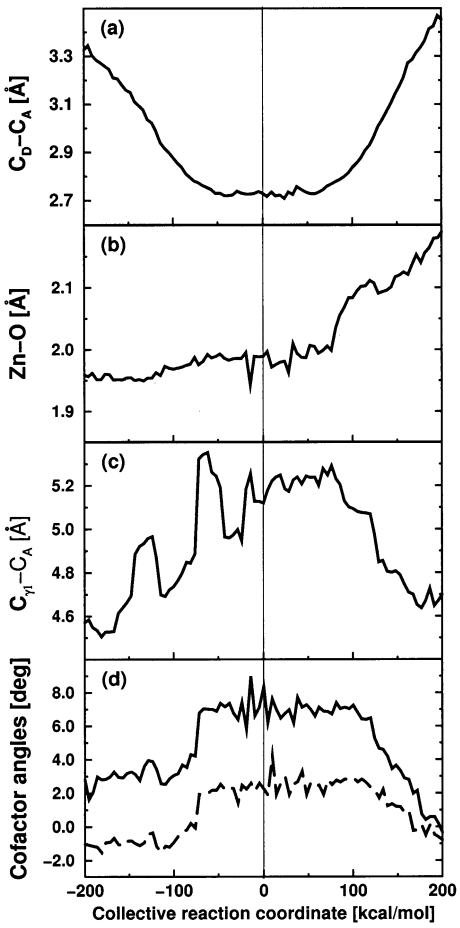

FIGURE 6: Equilibrium averages of geometrical properties along the collective reaction coordinate for LADH. (a) Donor−acceptor distance, (b) zinc−oxygen distance, (c) Val-203 $C_{\gamma 1}$−acceptor distance, and (d) C (solid) and N (dashed) NAD^+/NADH out-of-plane ring angles.

These simulations provide an explanation for the experimental observation that replacing Val-203 with the smaller residue alanine decreases the rate (*40*). (Note that these experimental results are not definitive due to the quantities measured and the complexity of the reaction.) We found that the distance between Val-203 and the reactive center significantly affects the activation free energy but is not correlated to the degree of barrier recrossing. Thus, the impact of the mutation on the enzyme activity is due to the alteration of the equilibrium free energy difference between the transition state and the reactant rather than nonequilibrium dynamical factors. Our results indicate that the motion of the acceptor carbon away from Val-203 and toward the donor carbon is a critical component of the reaction coordinate. These simulations also suggest that the motion of Val-203 directs the acceptor carbon toward the donor carbon through steric interactions involving the C_γ atoms of Val-203. When Val-203 is replaced with alanine, the C_γ atoms of Val-203

are no longer available for these steric interactions, leading to a decrease in the rate of hydride transfer.

Dihydrofolate Reductase

Dihydrofolate reductase (DHFR) catalyzes the conversion of dihydrofolate (DHF) to tetrahydrofolate (THF). This enzyme is essential for the maintenance of tetrahydrofolate levels needed to support the biosynthesis of purines, pyrimidines, and amino acids. As a result, DHFR has been favored as a pharmacological target. The kinetics of this enzymatic reaction have been studied extensively with experimental methods (*41*, *42*). The mechanism of DHFR has also been studied with a variety of theoretical methods (*15*, *43*, *44*).

The hybrid approach described above has been applied to the DHFR-catalyzed hydride transfer reaction depicted in Figure 2b (*16*, *19*). N5 of the substrate is assumed to be protonated prior to the hydride transfer. Thus, the hydride is transferred from NADPH to the protonated DHF to form the products $NADP^+$ and THF. As in the case of LADH, the classical and adiabatic quantum free energy profiles were calculated as functions of the collective reaction coordinate, and the experimental free energy of reaction and free energy of activation were reproduced by fitting two EVB parameters. For this system, the adiabatic quantum activation free energy is 2.4 kcal/mol lower than the classical activation free energy, indicating the significance of nuclear quantum effects. The transmission coefficient for DHFR-catalyzed hydride transfer was calculated to be 0.80, which is lower than the transmission coefficient of 0.95 calculated for the LADH-catalyzed reaction. This difference implies that dynamical barrier recrossings are more important for the DHFR reaction than for the LADH reaction.

Three-dimensional X-ray crystallographic structures have been determined for *Escherichia coli* DHFR in numerous substrate, cofactor, and inhibitor complexes (*1*). These structures illustrate that the surface loop formed by residues 9−24 (denoted the Met-20 loop) adopts three different conformations (denoted closed, occluded, and open) during the catalytic cycle. When the DHFR substrate and NADPH coenzyme are bound, the closed conformation is adopted. This closed conformation is stabilized by hydrogen bonding interactions between the Met-20 loop and the βF−βG loop (residues 117−131). These structural changes suggest that enzymatic motion plays a role in this reaction.

NMR relaxation experiments provide further insight into the changes in backbone dynamics during the catalytic cycle (*2*−*4*). NMR experiments on three different DHFR complexes suggest that the binding of the substrate and coenzyme alters the motion of the enzyme in regions far from the binding sites (including the Met-20 and βF−βG loops), as well as in the active site. Further support of this premise has arisen from classical molecular dynamics simulations on three different DHFR complexes (*15*). In these simulations, strong correlated and anticorrelated side chain motions involving spatially distinct protein regions (again including the Met-20 and βF−βG loops) were observed for the complex with DHF but not for the complexes with THF.

A genomic analysis for sequence conservation across 36 diverse species of DHFR from *E. coli* to human indicates that conserved residues are located throughout the enzyme

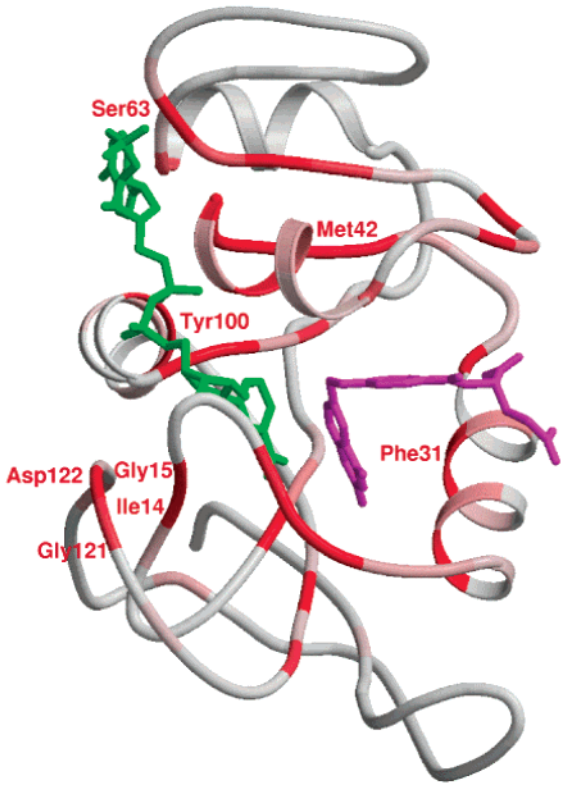

FIGURE 7: Three-dimensional structure of *E. coli* DHFR. The Met-20 and βF−βG loops, as well as the DHF substrate and NADPH coenzyme, are indicated. As in ref *16*, the residues conserved across numerous species from *E. coli* to human are indicated by a gradient color scheme (gray to red, where red is the most conserved). Residue numbers are given periodically for reference.

(*16*). Figure 7 summarizes the results of this genomic analysis. As illustrated in this figure, many of the conserved residues are in the active site and hence impact the binding of the substrate and coenzyme. On the other hand, several conserved residues are in distal regions of the enzyme (i.e., residues 41−43 and 121−123). Residues 122 and 15, which are hydrogen bonded in the closed conformation of the Met-20 loop, are absolutely conserved. Although some of these distal residues may be conserved for structural purposes, others may be conserved to preserve certain types of motion of the enzyme during catalysis.

Kinetic measurements of mutant DHFR enzymes suggest that distal regions of the enzyme strongly influence the hydride transfer reaction. For example, when Gly-121 was replaced with valine, the rate of hydride transfer was found to decrease by a factor of 163. As shown in Figure 7, Gly-121 is located on the exterior of the enzyme and is ∼10 Å from the active site. Furthermore, double mutations involving Gly-121 and Met-42 (residues that are distal to the active site and separated by ∼19 Å) were found to exhibit nonadditivity effects (*16*). This nonadditivity suggests a coupling of the βF−βG loop to distant regions of the enzyme. Note that site-specific mutagenesis does not distinguish between nonadditivity effects resulting from changes in conformation and those effects resulting from changes in molecular motions.

We used our hybrid simulations to further investigate the role of motion in the DHFR reaction. This hybrid approach was used to perform a systematic study of more than 200 distances involving conserved residues. We investigated the

impact of these motions on the free energy of activation and the degree of barrier recrossing. On the basis of experimental kinetic measurements of hydride transfer in DHFR, the thermally averaged promoting motions were determined to occur on the millisecond time scale. As discussed above, the overall mechanism and rate of catalysis are expected to be influenced more by the promoting motions occurring on the millisecond time scale than by the dynamical motions occurring on the femtosecond time scale. Nevertheless, the combination of both types of analyses provides insight into the detailed mechanism of the enzyme motion.

Figure 8 illustrates selected thermally averaged geometrical properties along the collective reaction coordinate for the DHFR-catalyzed reaction. Figure 8a shows that the donor−acceptor distance decreases from 3.4 to 2.7 Å as the reaction evolves from the reactant to the transition state. In addition, Figure 8b shows that the angle between the acceptor carbon and the methylene amino linkage in DHF increases from 114° to 117° as the reaction evolves from the reactant to the transition state. (This angle is indicated by the yellow arc in Figure 9.) The motions of amino acid residues in the active site relative to the coenzyme and substrate are also important. For example, as shown in Figure 8d, the distance between C_ζ of Phe-31 and C11 of DHF decreases by ~1 Å as the reaction evolves from the reactant to the transition state. As Phe-31 moves closer to the substrate, the angle between the acceptor carbon and the methylene amino linkage in DHF increases and the donor−acceptor distance decreases, suggesting that the Phe-31 motion may direct these changes. Note that Phe-31 is tightly conserved, and mutations of this residue have been found to significantly decrease the rate of hydride transfer. The motion of Ile-14 and Tyr-100 shown in Figure 8f may provide similar direction from the donor side. A more unexpected result is that the motion of a residue on the exterior of the enzyme was found to be important for catalysis. Specifically, the motion of Asp-122 relative to Gly-15 was found to contribute to the reaction coordinate. Figure 8e illustrates that the hydrogen bond between these two residues increases by ~0.4 Å as the reaction evolves from the reactant to the transition state. In contrast, this figure shows that the hydrogen bond distance between Ile-14 and the NADPH coenzyme is nearly constant (~2.95 Å) as the reaction evolves from the reactant to the transition state. (Note that these hydrogen bonding motions are susceptible to sampling difficulties arising from metastable states in these simulations.) As Gly-15 moves away from Asp-122, the donor−acceptor distance decreases, suggesting that the neighboring residue, Ile-14, which is hydrogen-bonded to the NADPH, may direct the donor toward the acceptor. Note that Asp-122, Gly-15, and Ile-14 are all absolutely conserved residues, and mutations of Gly-121 and Asp-122 have been found to significantly decrease the rate of hydride transfer.

This analysis supports the hypothesis of a network of coupled promoting motions in DHFR (*16*). The residues participating in this network are both in the active site and distal to the active site. A portion of this network is illustrated in Figure 9. Note that this network is most likely not complete or unique. In addition, this analysis is unable to differentiate between motions playing an active role in catalysis and motions responding to alterations caused by catalysis. Nevertheless, all of these systematic changes in thermally averaged properties occur along the same collective reaction coordinate representing hydride transfer. This type of network has broad implications for protein engineering because of the consequences arising from the interruption of coupled motions.

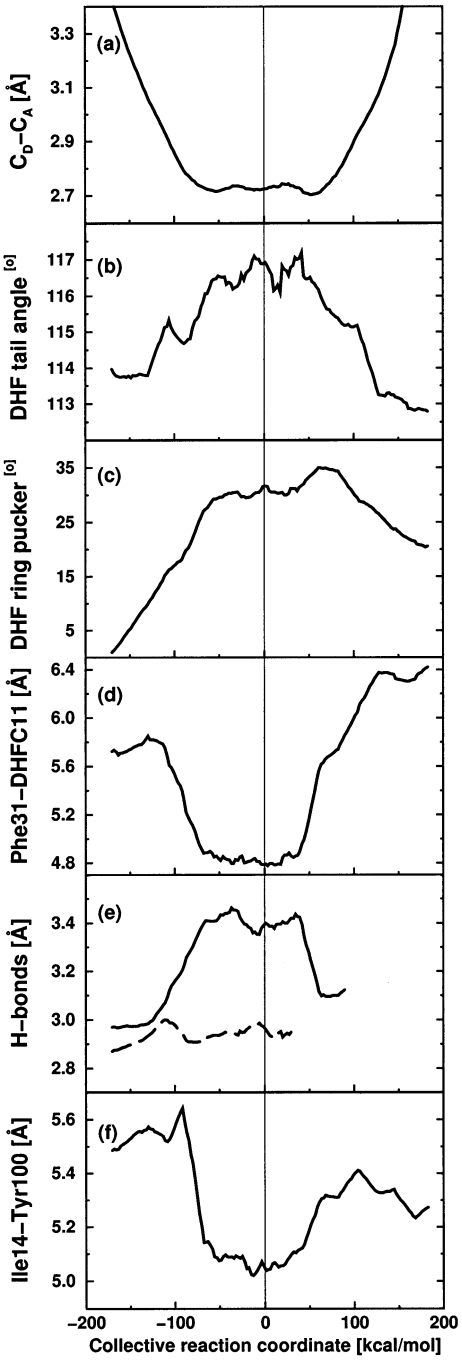

FIGURE 8: Equilibrium averages of geometrical properties along the collective reaction coordinate for DHFR. (a) Donor−acceptor distance, (b) angle between the acceptor and methylene amino linkage in DHF, (c) DHF pterin ring puckering angle, (d) distance between C_ζ of Phe-31 and C11 of DHF, (e) hydrogen bonding distance between an N atom of Asp-122 and an O atom of Gly-15 (solid) and between an O atom of Ile-14 and a carboxamide N atom of NADPH (dashed), and (f) distance between C_δ of Ile-14 and the side chain oxygen of Tyr-100.

Conclusions

A wealth of experimental and theoretical data indicates that enzyme motion plays a vital role in enzyme activity.

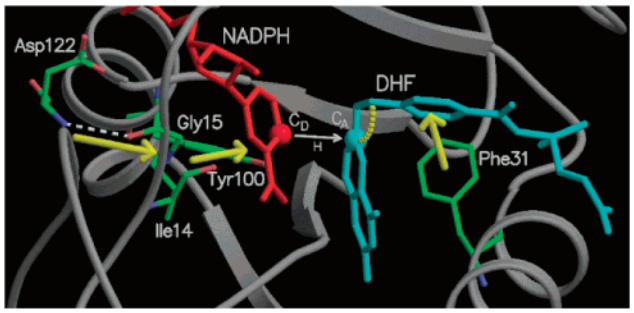

FIGURE 9: Diagram of a portion of the network of coupled promoting motions in DHFR. The yellow arrows and arc indicate the coupled promoting motions.

This review distinguishes between two different types of motion. Promoting motions are defined as systematic changes in thermally averaged properties along the collective reaction coordinate (i.e., as the reaction evolves from the reactant to the transition state to the product). Dynamical motions are defined as geometrical properties that are correlated to the degree of barrier recrossing. Promoting motions are expected to have a greater impact on enzyme activity than dynamical motions for two main reasons. First, promoting motions occur on the time scale of the catalyzed chemical reaction, while dynamical motions typically occur on a much faster time scale. Second, promoting motions influence the activation free energy barrier, which contributes to the exponential of the rate expression, while dynamical motions influence the transmission coefficient, which is a prefactor in the rate expression. These promoting motions reflect conformational changes that occur during the catalyzed chemical reaction.

A hybrid theoretical approach has been developed to investigate motion in enzymatic reactions. The promoting motions are studied with a series of equilibrium simulations along the collective reaction coordinate, while the dynamical motions are studied with real-time, dynamical trajectories initiated at the transition state. The application of this hybrid approach to hydride transfer in LADH and DHFR has resulted in the identification and characterization of important enzyme motions. The application to DHFR has led to the proposal of a network of coupled promoting motions in enzymatic reactions. One hypothesis is that thermal fluctuations lead to directed motions through this network.

Despite recent experimental and theoretical advances, the mechanistic role of motion in enzymatic reactions is still not well understood. Structural studies indicate the required conformational changes. The hybrid theoretical studies discussed in this review provide information about the changes in thermally averaged properties along a collective reaction coordinate. Further insight may be gained by studying the instantaneous normal modes of the enzyme for configurations along the collective reaction coordinate. Of particular interest are normal modes on the time scale of the catalyzed chemical reaction or with strong components from the donor−acceptor vibration. In addition to studies of wild-type enzymes, further insight into enzyme motions may be obtained by theoretical and experimental studies of mutant, heterodimer, and hybrid enzymes. The elucidation of the mechanistic role of motion in enzymatic reactions will have a substantial impact on protein engineering and drug design.

ACKNOWLEDGMENT

I owe great thanks to James Watney, Salomon Billeter, Pratul Agarwal, and Kim Wong for stimulating discussions and creation of the figures.

REFERENCES

1. Sawaya, M. R., and Kraut, J. (1997) *Biochemistry 36*, 586−603.
2. Epstein, D. M., Benkovic, S. J., and Wright, P. E. (1995) *Biochemistry 34*, 11037−11048.
3. Osborne, M. J., Schnell, J., Benkovic, S. J., Dyson, H. J., and Wright, P. E. (2001) *Biochemistry 40*, 9846−9859.
4. Falzone, C. J., Wright, P. E., and Benkovic, S. J. (1994) *Biochemistry 33*, 439−442.
5. Li, L., Falzone, C. J., Wright, P. E., and Benkovic, S. J. (1992) *Biochemistry 31*, 7826−7833.
6. Miller, G. P., and Benkovic, S. J. (1998) *Biochemistry 37*, 6336−6342.
7. Cameron, C. E., and Benkovic, S. J. (1997) *Biochemistry 36*, 15792−157800.
8. Huang, Z., Wagner, C. R., and Benkovic, S. J. (1994) *Biochemistry 33*, 11576−11585.
9. Wagner, C. R., Huang, Z., Singleton, S. F., and Benkovic, S. J. (1995) *Biochemistry 34*, 15671−15680.
10. Mildvan, A. S., Weber, D. J., and Kuliopulos, A. (1992) *Arch. Biochem. Biophys. 294*, 327−340.
11. Karplus, M. (2000) *J. Phys. Chem. B 104*, 11−27.
12. Young, L., and Post, C. B. (1996) *Biochemistry 35*, 15129−15133.
13. Villa, J., and Warshel, A. (2001) *J. Phys. Chem. B 105*, 7887−7907.
14. Antoniou, D., and Schwartz, S. D. (2001) *J. Phys. Chem. B 105*, 5553−5558.
15. Radkiewicz, J. L., and Brooks, C. L. (2000) *J. Am. Chem. Soc. 122*, 225−231.
16. Agarwal, P. K., Billeter, S. R., Rajagopalan, P. T. R., Benkovic, S. J., and Hammes-Schiffer, S. (2002) *Proc. Natl. Acad. Sci. U.S.A. 99*, 2794−2799.
17. Billeter, S. R., Webb, S. P., Iordanov, T., Agarwal, P. K., and Hammes-Schiffer, S. (2001) *J. Chem. Phys. 114*, 6925−6936.
18. Billeter, S. R., Webb, S. P., Agarwal, P. K., Iordanov, T., and Hammes-Schiffer, S. (2001) *J. Am. Chem. Soc. 123*, 11262−11272.
19. Agarwal, P. K., Billeter, S. R., and Hammes-Schiffer, S. (2002) *J. Phys. Chem. B 106*, 3283−3293.
20. Warshel, A. (1991) *Computer Modeling of Chemical Reactions in Enzymes and Solutions*, John Wiley & Sons, New York.
21. Webb, S. P., and Hammes-Schiffer, S. (2000) *J. Chem. Phys. 113*, 5214−5227.
22. Iordanov, T., Billeter, S. R., Webb, S. P., and Hammes-Schiffer, S. (2001) *Chem. Phys. Lett. 338*, 389−397.
23. Wigner, E. (1937) *J. Chem. Phys. 5*, 720−725.
24. Neria, E., and Karplus, M. (1996) *J. Chem. Phys. 105*, 10812−10818.
25. Marcus, R. A. (1964) *Annu. Rev. Phys. Chem. 15*, 155−196.
26. Keck, J. C. (1960) *J. Chem. Phys. 32*, 1035−1050.
27. Anderson, J. B. (1973) *J. Chem. Phys. 58*, 4684−4692.
28. Bennett, C. H. (1997) *Algorithms for Chemical Computation*, American Chemical Society, Washington, DC.
29. Tully, J. C. (1990) *J. Chem. Phys. 93*, 1061−1071.
30. Hammes-Schiffer, S. (1998) *J. Phys. Chem. A 102*, 10443−10454.
31. Bahnson, B. J., Park, D. H., Kim, K., Plapp, B. V., and Klinman, J. P. (1993) *Biochemistry 32*, 5503−5507.
32. Bahnson, B. J., and Klinman, J. P. (1995) *Methods Enzymol. 249*, 373−397.
33. Rucker, J., and Klinman, J. P. (1999) *J. Am. Chem. Soc. 121*, 1997−2006.
34. Luo, J., Kahn, K., and Bruice, T. C. (1999) *Bioorg. Chem. 27*, 289−296.
35. Luo, J., and Bruice, T. C. (2001) *J. Am. Chem. Soc. 123*, 11952−11959.
36. Alhambra, C., Corchado, J. C., Sanchez, M. L., Gao, J. L., and Truhlar, D. G. (2000) *J. Am. Chem. Soc. 122*, 8197−8203.
37. Alhambra, C., Corchado, J., Sanchez, M. L., Garcia-Viloca, M., Gao, J., and Truhlar, D. G. (2001) *J. Phys. Chem. B 105*, 11326−11340.

38. Cui, Q., Elstner, M., and Karplus, M. (2002) *J. Phys. Chem. B 106*, 2721−2740.
39. Agarwal, P. K., Webb, S. P., and Hammes-Schiffer, S. (2000) *J. Am. Chem. Soc. 122*, 4803−4812.
40. Bahnson, B. J., Colby, T. D., Chin, J. K., Goldstein, B. M., and Klinman, J. P. (1997) *Proc. Natl. Acad. Sci. U.S.A. 94*, 12797−12802.
41. Fierke, C. A., Johnson, K. A., and Benkovic, S. J. (1987) *Biochemistry 26*, 4085−4092.
42. Miller, G. P., and Benkovic, S. J. (1998) *Chem. Biol. 5*, R105−R113.
43. Cummins, P. L., and Gready, J. E. (2001) *J. Am. Chem. Soc. 123*, 3418−3428.
44. Castillo, R., Andres, J., and Moliner, V. (1999) *J. Am. Chem. Soc. 121*, 12140−12147.

BI0267137